International Journal of Applied Earth Observation and Geoinformation 38 (2015) 335–348

Contents lists available at ScienceDirect

International Journal of Applied Earth Observation and Geoinformation

journal homepage: www.elsevier.com/locate/jag

Monitoring levels of cyanobacterial blooms using the visual cyanobacteria index (VCI) and floating algae index (FAI)

Yoichi Oyama[a,*], Takehiko Fukushima[a], Bunkei Matsushita[a], Hana Matsuzaki[b], Koichi Kamiya[a,c], Hisao Kobinata[c]

[a] Faculty of Life and Environmental Sciences, University of Tsukuba, 1-1-1 Tennoudai, Tsukuba-City, Ibaraki 305-8572, Japan
[b] Graduate School of Frontier Sciences, The University of Tokyo, 5-1-5 Kashiwanoha, Kashiwa-City, Chiba 277-8563, Japan
[c] Ibaraki Kasumigaura Environmental Science Center, 1853 Okijyuku, Tsuchiura-City, Ibaraki 300-0023, Japan

ARTICLE INFO

Article history:
Received 14 October 2014
Received in revised form 4 February 2015
Accepted 6 February 2015
Available online 17 February 2015

Keywords:
Cyanobacterial blooms
Landsat
Lake
Chlorophyll-a
Phycocyanin
Water amenity

ABSTRACT

Cyanobacterial bloom is a growing environmental problem in inland waters. In this study, we propose a method for monitoring levels of cyanobacterial blooms from Landsat/ETM+ images. The visual cyanobacteria index (VCI) is a simple index for in-situ visual interpretation of cyanobacterial blooms levels, by classifying them into six categories based on aggregation (e.g., subsurface blooms, surface scum). The floating algae index (FAI) and remote sensing reflectance in the red wavelength domain, which can be obtained from Landsat/ETM+ images, were related to the VCI for estimating cyanobacteria bloom levels from the Landsat/ETM+ images. Nine field campaigns were carried out at Lakes Nishiura and Kitaura (Lake Kasumigaura group), Japan, from June to August 2012. We also collected reflectance spectra at 20 stations for different VCI levels on August 3, 2012. The reflectance spectra were recalculated in correspondence to each ETM+ band, and used to calculate the FAI. The FAI values were then used to determine thresholds for classifying cyanobacterial blooms into different VCI levels. These FAI thresholds were validated using three Landsat/ETM+ images. Results showed that FAI values differed significantly at the respective VCI levels except between levels 1 and 2 (subsurface blooms) and levels 5 and 6 (surface scum and hyperscum). This indicated that the FAI was able to detect the high level of cyanobacteria that forms surface scum. In contrast, the Landsat/ETM+ band 3 reflectance could be used as an alternative index for distinguishing surface scum and hyperscum. Application of the thresholds for VCI classifications to three Landsat/ETM+ images showed that the volume of cyanobacterial blooms can be effectively classified into the six VCI levels.

1. Introduction

Eutrophication is a common and growing environmental problem in lakes, rivers, estuaries, and coastal oceans (Smith and Schindler, 2009). In particular, excessive input of nutrients as a consequence of human activity has resulted in the dominance of colony-forming species of cyanobacteria in water bodies (Dokulil and Teubner, 2000). Cyanobacterial blooms have various negative impacts on water resources used for drinking, agricultural, industrial, commercial and recreational purposes (Carpenter et al., 1998; Song et al., 2014). According to the research on U.K. freshwater lakes, annual economic loss due to eutrophication is more than $100 million per year^{-1} (Pretty et al., 2003). In addition, cyanobacterial toxins (cyanotoxins) are widely recognized as a hazard to human and animal health (Bartram et al., 1999; Codd, 2000).

Conventional water quality monitoring has been based on traditional ship surveys and laboratory measurements. However, it is very difficult to observe cyanobacterial blooms from ship surveys due to the patchiness and high spatial and temporal variability of the blooms. Satellite remote sensing provides more reliable information about the extent of cyanobacterial blooms than traditional surveys (Blondeau-Patissier et al., 2014). Algorithms for estimating chlorophyll-a (Chl-a) concentration have been applied to monitor cyanobacterial blooms, because high Chl-a concentration is an index of the presence of blooms (Subramaniam et al., 2002; Kutser, 2004; Lobo et al., 2009). Phycocyanin, which is a specific pigment of cyanobacteria, is also used as a proxy for cyanobacterial blooms (Vincent et al., 2004; Simis et al., 2005; Dash et al., 2011; Mishra and Mishra, 2014). In addition, several studies have reported using different algorithms for the purpose of detecting

* Corresponding author. Tel.: +81 29 853 7189; fax: +81 29 853 7189.
E-mail address: y-oyama@ies.life.tsukuba.ac.jp (Y. Oyama).

http://dx.doi.org/10.1016/j.jag.2015.02.002
0303-2434/

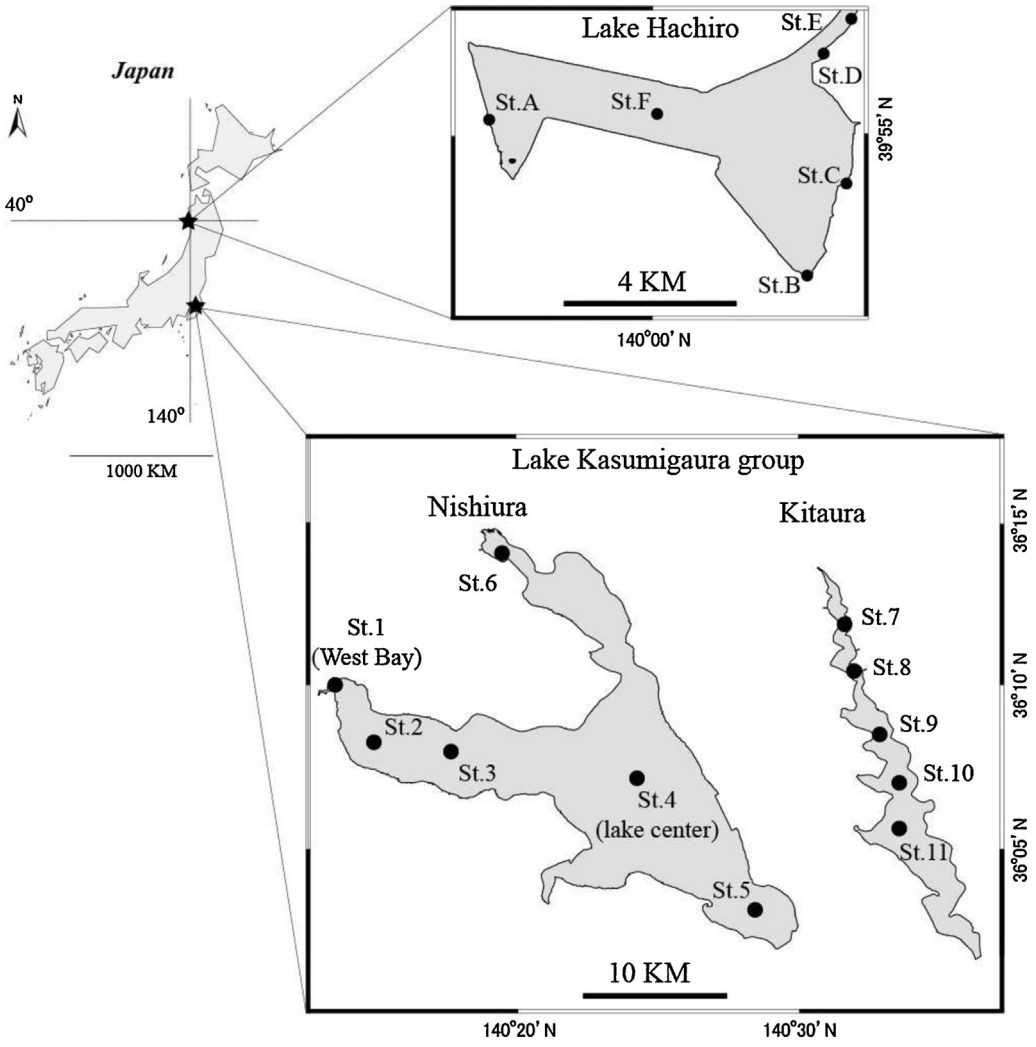

Fig. 1. Observation points in Lakes Hachiro, Nishiura, and Kitaura, Japan.

cyanobacterial blooms: a single band (Kahru et al., 1994 McKinna et al., 2011); the normalized difference vegetation index (NDVI) and the enhanced vegetation index (EVI) (Hu and He, 2008); linear baseline algorithms such as the maximum chlorophyll index (MCI; Gower et al., 2005); the cyanobacteria index (CI; Wynne et al., 2008); the floating algae index (FAI; Hu, 2009); and the maximum peak height (MPH) algorithm (Matthews et al., 2012; Matthews, 2014).

However, most of these algorithms for cyanobacterial blooms cannot provide information on quantity in cases of surface accumulation (surface scum and dense mats). This is because the scum is optically opaque, and therefore the satellite sensor cannot get any information about water properties below the scum (Kutser, 2004). The spectral signals of the scum are characterized by higher reflectance in the near-infrared (NIR) region than in other wavelength regions due to the decrease of absorption by the water itself. This spectral feature leads to the failure of algorithms that estimate Chl-a and phycocyanin concentration by relying on the characteristics of water absorption in the NIR (Ruiz-Verdú et al., 2008; Duan et al., 2012). The linear baseline algorithms for MERIS (medium resolution imaging spectrometer) images such as MCI, CI and MPH have the same problem. This is because reflectance at the NIR region is used to delineate the baseline for calculating the height of the Chl-a fluorescence peak. Matthews et al. (2012) reported that the Chl-a fluorescence peak shifts toward a 750 nm or higher wavelength in the extremely high biomass conditions associated with surface scum. The FAI, another linear baseline algorithm based on MODIS (moderate resolution imaging spectroradiometer) images, is less influenced by the decreased absorption of water in the NIR region compared to these other algorithms. This is because the FAI baseline is delineated using the reflectance at short-wave infrared (SWIR) regions instead of the NIR region. However, the relation between the FAI and the extent of the cyanobacterial blooms is not clear.

In addition, in-situ sampling procedures for measuring pigment concentrations in cyanobacterial blooms may also influence the development and validation of a Chl-a or phycocyanin algorithm. Kutser (2004) pointed out that special precautions are needed to collect aggregations of cyanobacteria from the layer just below the water surface, or from mats floating on the surface. Concentration often depends on sampling volume, because current sampling devices cannot collect an aggregation of cyanobacteria while separating out the rest of the subsurface water. Aggregation is mixed and diluted in the sampling devices, causing underestimation of the concentration of Chl-a or phycocyanin measured in the laboratory. Therefore, alternative measurement approaches are needed for evaluating the volume of surface cyanobacterial blooms using satellite data.

Aizaki et al. (1995a) investigated the relationship between observers' impressions of lake scenery and the extent of cyanobacterial blooms using a questionnaire with photographs of different aggregations of cyanobacteria (patches, scums, and mats) in Lake

Nishiura (west part of Lake Kasumigaura), Japan. From the results, they developed a new environmental indicator of cyanobacterial blooms called the visual cyanobacteria index (VCI) (see Appendix A). They classified profusion of cyanobacterial blooms into six levels of aggregation based on visual appearance. Since the satellite signals from a body of water are also influenced by optical properties, the VCI has the potential to be an alternative indicator for monitoring cyanobacterial blooms using satellite remote sensing.

The objectives of this study were to: (1) investigate the relationships between spectral signatures and VCI levels based on in-situ observations; (2) develop a method for applying VCI to Landsat images based on FAI thresholds; and (3) validate the method using three Landsat images.

2. Method

2.1. Study sites

Three Japanese lakes were selected for the investigation of pigment concentrations and spectral characteristics in cyanobacterial blooms at each VCI level, as well as the applicability of the VCI to Landsat images (Fig. 1). The first two were Lakes Nishiura and Kitaura. Lake Nishiura is a main part of the Lake Kasumigaura group, with a surface area of 171 km^2 and an average depth of 3.4 m. Lake Kitaura has a surface area of 34 km^2 and an average depth of 4.5 m. Massive cyanobacterial blooms of *Microcystis* sp. occurred in these lakes from the early 1970s through the late 1990s, then reappeared in 2011. The third lake was Lake Hachiro, located in the northern part of Japan. This lake was the second largest lake in Japan (222 km^2 in surface area) until 1957, when the surface area was reduced to approximately one-fifth (49 km^2) due to reclamation (Sato, 1990). Because of the high nutrient loads from the reclamation area and the shallow water depth (average depth 2.8 m), cyanobacterial blooms have been a major concern in this lake.

2.2. Field investigations

Eight field investigations were carried out at Lakes Nishiura and Kitaura (Lake Kasumigaura group) from June to August 2012 when cyanobacterial blooms occurred in the lakes (i.e., June 19 and 30; July 4, 11 and 19; and August 1, 9 and 21). For each investigation, we divided the general term "cyanobacterial blooms" into three conditions: (1) subsurface bloom (VCI levels 1 and 2; see Fig. A.1(a) and (b)); surface scum (VCI levels 3–5; see Fig. A.1(c)–(e)); and hyperscum (VCI level 6; see Fig. A.1(f)). Water samples were randomly collected at each of the 11 stations during the study period (Fig. 1). The samples were collected using with a clear cylinder sampler (15 cm diameter, 50 cm length), which was slowly lowered into the water to minimize disturbance of the cyanobacterial blooms. The sampling volume was kept constant at all stations (from the surface to a depth of 20 cm) as concentration of cyanobacteria can easily change with sampling volume when aggregation is heavy on the water surface. Levels of cyanobacterial bloom were simultaneously recorded using the photographs of the VCI (Fig. A.1).

The water samples were brought back to the laboratory to measure Chl-a concentration using a spectrophotometric method (SCOR-UNESCO, 1966), and phycocyanin concentration using a fluorometric method (Hino and Takano, 1995). The water sample was first filtered onto a Whatman GF/F glass–fiber filter (47 mm diameter, 0.7 μm pore size) to collect the cyanobacterial particles. Methanol (100%) and a phosphate buffer solution (pH 7.0, 1/15 mol L^{-1}) were used to extract Chl-a and phycocyanin, respectively. The extracts were left to sit in the dark at 4 °C for 24 h. They were then centrifuged at 3000 rpm for 5 min immediately before analysis. The Chl-a concentration was analyzed using a spectrophotometer (UV-1600, Shimadzu, Kyoto, Japan). The optical density (OD) of the extract was measured at four wavelengths: 750, 663, 645 and 630 nm, and Chl-a concentrations were calculated using SCOR-UNESCO equations (SCOR-UNESCO, 1966). Phycocyanin concentration was analyzed using a spectrofluorometer (F-4500, Hitachi, Kyoto, Japan). The fluorescence emission spectrum of the phycocyanin was measured at a wavelength between 600 and 700 nm at an excitation of 630 nm. A c-phycocyanin from *Spirulina* sp. powder (Sigma–Aldrich, MO) was used to produce the standard solution of the phycocyanin. The area of fluorescence peak around 660 nm was calculated and used to measure the phycocyanin concentration of water samples from those of the standard solutions. For each sampling point, triplicate samples were made for Chl-a and phycocianin measurements, respectively, and the averaged values were used for the next analyses.

One special field campaign was carried out during 9:00 AM and 12:00 AM on August 3, 2012 at the west bay of Lake Nishiura (around St. 1 in Fig. 1). In addition to Chl-a concentration, phycocyanin concentration, and recording cyanobacterial bloom levels by the VCI photographs, water-leaving reflectance values were measured following the Method 1 described by Mueller et al. (2000) using a FieldSpec FR spectroradiometer (Analytical Spectral Devices, Boulder, CO; instantaneous field of view (IFOV) of 25°, wavelengths range from 350 to 2500 nm, spectral resolutions are 1.4 nm for 350–1050 nm and 2.0 nm for 1000–2500 nm). The upwelling radiance (L_u) (W m^{-2} sr^{-1}), the downwelling radiance (L_d) (W m^{-2} sr^{-1}), and the skylight radiance (L_{sky}) (W m^{-2} sr^{-1}) were measured at a nadir or zenith angle of 42° with a azimuth angle about 140° to the solar plane. A SRT-99-100 Spectralon reflectance panel (Labsphere, NH) was used for the L_d measurements. The measurements are internally resampled by the instrument to 1 nm intervals. While the measurements were being taken, the weather was clear with almost no wind (approximately 0 m s^{-1}). In total, the spectral measurements were collected from 20 sites in time with different levels of cyanobacterial bloom. The L_u and L_{sky} were converted according to the respective ETM+ radiances, $L_{u,Bi}$ and $L_{sky,Bi}$, using the following equation:

$$L_{u,Bi} \text{or} L_{sky,Bi} = \frac{\Sigma_m^n (L(\lambda) \times \mathrm{SRF}(\lambda))}{\Sigma_m^n \mathrm{SRF}(\lambda)} \quad (1)$$

where L is the measured spectral radiance (i.e., L_u, or L_{sky}) (W m^{-2} sr^{-1}), λ is the wavelength (nm), Bi is the ETM+ ith band, SRF is the spectral response function for each ETM+ band, and m and n are the start and end wavelengths of the SRF for each ETM+ band, respectively. Since the L_d was measured via the Spectralon reflectance panel, the ETM+ downwelling radiance ($L_{d,Bi}$) was recalculated by the following equation:

$$L_{d,Bi} = \frac{\Sigma_m^n (L(\lambda) \times \mathrm{Cal}(\lambda) \times \mathrm{SRF}(\lambda))}{\Sigma_m^n \mathrm{SRF}(\lambda)} \quad (2)$$

where Cal is the calibration factor for the Spectralon reflectance panel. Finally, the in-situ ETM+ radiances were used to calculate the in-situ ETM+ reflectance ($R_{in\text{-}situ}$) by the following equation:

$$R_{in-situ,Bi} = \left(\frac{L_{u,Bi} - rL_{sky,Bi}}{L_{d,Bi}} \right) \quad (3)$$

where r is the ratio of surface reflection determined as a function of wind speed. We used a value of 0.022 as the r value (Mobley, 1999).

2.3. Landsat images

Three Landsat/ETM+ images were acquired from the USGS Earth Explorer website (http://earthexplorer.usgs.gov/): one of Lakes Nishiura and Kitaura (path/row: 107/35) on August 21, 2012 (coinciding with the eighth field investigation in the two lakes), and the

others of Lake Hachiro (path/row: 108/32) on August 28, 2012, and September 13, 2012 (coinciding with two field investigations in the lake by the environmental office for Lake Hachiro, Akita Prefecture). The Landsat/ETM+ was launched on the April 15, 1999, and has been monitoring the earth's surface with a repeat cycle of 16 days. However, the images have had wedge-shaped gaps since May 31, 2003, due to the failure of the scan-line corrector (SLC) of the ETM+ sensor. Although approximately 22% of the image area is missing, radiometric and geometric quality of the images have been the same after the SLC failure as they were before (Storey et al., 2005). The ETM+ sensor has five bands in visible and NIR wavelengths (band 1: 450–520 nm; band 2: 530–610 nm; band 3: 630–690 nm; band 4: 750–900 nm; band 8: 520–900 nm), two bands in SWIR wavelengths (band 5: 1550–1570 nm; band 7: 2090–2350 nm), and one band in the thermal infrared wavelength (band 6: 10,400–12500 nm). The 30 m spatial resolution of ETM+ bands 1–5 and 7 are required to monitor small inland waters.

The digital numbers (DNs) of ETM+ were first converted to satellite-derived radiance (L_{sat}) using the following equation:

$$L_{sat,Bi} = DN_{Bi} \times \frac{(L_{max,Bi} - L_{min,Bj})}{(QCal_{max,Bi} + QCal_{min,Bi})} - L_{min,Bi} \quad (4)$$

where L_{max} and L_{min} represent the dynamic range of the ETM+ sensor, and $Qcal_{max}$ and $Qcal_{min}$ are the maximum and minimum quantized calibrated pixel values (typically 255 and 1, respectively). The radiance values were then converted to satellite-derived reflectance with correction of atmospheric noises such as Rayleigh scattering and absorption by air molecules, and aerosol scattering and absorption. Atmospheric correction was carried out using a radiative transfer code 6S (Vermote et al., 1997). The major input parameters of the 6S are geometric location (latitude, longitude, altitude), atmospheric and aerosol models, and horizontal visibility. We used the standard conditions (the middle latitude summer atmospheric model, the maritime aerosol model) proposed by the 6S code. Horizontal visibilities near the three lakes for the respective acquisition date of the Landsat/ETM+ images were obtained from a website of the Japan Meteorological Agency (http://www.jma.go.jp/jma/index.html). The calculated reflectance is called the 6S-corrected reflectance (R_{6S}).

2.4. FAI of the index for detecting cyanobacterial blooms

We selected the FAI (Hu, 2009) for detecting cyanobacterial blooms from the Landsat images. The advantage of the FAI is that it is less sensitive to changes in environmental and observational conditions (e.g., solar/viewing geometry, and sun glint) than the NDVI or EVI (Hu, 2009). Although the FAI was originally developed for MODIS images, it can also be derived from reflectance in ETM+ bands 3, 4, and 5 using the following linear baseline algorithm:

$$FAI = R_{B4} - \left[R_{B3} + (R_{B5} - R_{B3}) \times \frac{(\lambda_{B4} - \lambda_{B3})}{(\lambda_{B5} - \lambda_{B3})}\right] \quad (5)$$

where R is the reflectance, and λ_{Bi} is the center wavelength for the ETM+ ith band (i.e., λ_{B3} = 660 nm, λ_{B4} = 825 nm, and λ_{B5} = 1650 nm). We calculated the FAI using the in-situ ETM+ reflectance ($R_{in\text{-}situ}$) and the 6S-corrected (satellite-derived) reflectance (R_{6S}), respectively. However, for the satellite data, the original FAI proposed by Hu (2009) was calculated from the Rayleigh-corrected reflectance (R_{rc}). This was because FAI calculated from R_{rc} is not comparable to that calculated from $R_{in\text{-}situ}$ in that the $R_{in\text{-}situ}$ is free not only from the Rayleigh scattering effect but also gaseous absorption, aerosol absorption and scattering effects.

2.5. Determination of FAI thresholds for each VCI level

Calculated FAIs were used to determine the thresholds for classification of the cyanobacterial blooms into the six VCI levels. First, in-situ FAI values were compared for different VCI levels, and thresholds of the FAI were determined. Second, these FAI thresholds were applied to three Landsat/ETM+ images. Third, a 3×3 window was applied to each sampling station. For Lakes Nishiura and Kitaura, pixels were extracted based on our seven sampling points on August 21, 2012. For Lake Hachiro, in-situ-observed VCI values and locations of observation points were obtained from a website of the environmental office for Lake Hachiro, Akita Prefecture (http://www.pref.akita.lg.jp/www/genre/0000000000000/1160459269368/index.html). This website has supplied information on cyanobacterial blooms observations in Lake Hachiro using the VCI since 2008, in which, two field investigations on August 28, 2012 and September 13, 2012 were timed to coincide with acquisition of Landsat/ETM+ images within ± 1.5 h. The extracted FAI values of the 3×3 window averaged and classified into the six VCI levels based on the thresholds determined by the in-situ FAI values. Finally, VCI levels were compared to in-situ data and Landsat/ETM+ images.

3. Results

3.1. Pigment concentrations and spectral characteristics in each VCI level

Fig. 2 shows the box-and-whisker plots of Chl-a and phycocyanin concentration in cyanobacterial blooms at each VCI level.

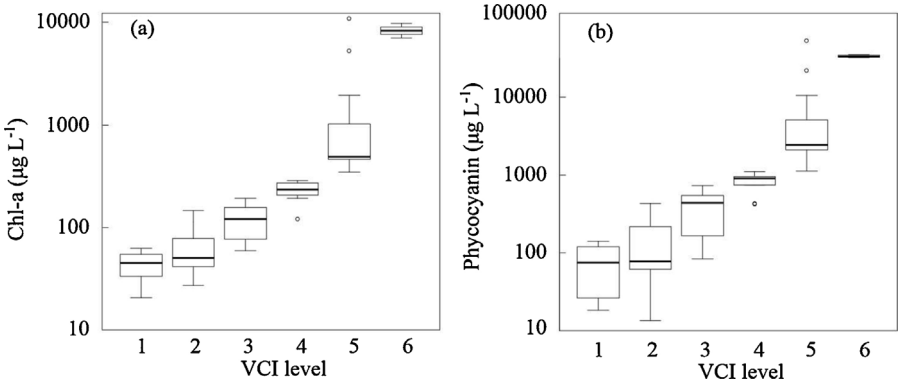

Fig. 2. (a) Chl-a, and (b) phycocyanin. The box-and-whisker plots of pigment concentrations in each VCI level were obtained from eight field investigations during June–August, 2012, in Lakes Nishiura and Kitaura (Lake Kasumigaura group) (N = 14, 12, 9, 10, 15 and 3 for VCI level 1, 2, 3, 4, 5, and 6, respectively). The vertical axis is expressed by log scale. **S**olid lines in the boxes represent the median value. The upper and lower fences represent the 1st and 3rd quartiles (Q1 and Q3), respectively. The lower and upper whiskers were calculated from (Q1 – 1.5 × IQR) and (Q3 **+** 1.5 × IQR), respectively, where IQR is the interquartile range represented by the width of the box (i.e., Q3–Q1). Data above or below the whisker were defined as the outliers and are shown as open circles.

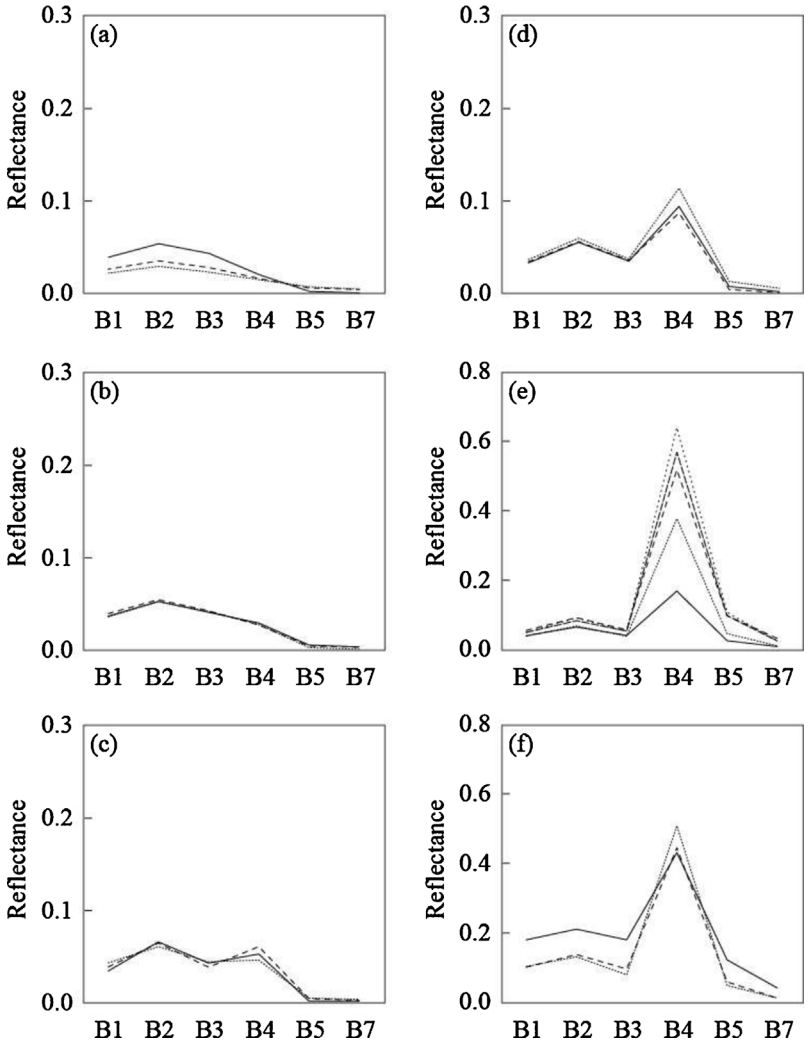

Fig. 3. The in-situ measured reflectance spectra for the respective VCI levels in Lake Nishiura collected on August 3, 2012: (a) Level 1; (b) level 2; (c) level 3; (d) level 4; (e) level 5; (f) level 6. The measured reflectances were recalculated to Landsat/ETM+ band reflectances. The scale of the vertical axis is different between (a–d) and (e–f).

The data were obtained from the observation of Lakes Nishiura and Kitaura during June-August, 2012. Both Chl-a and phycocyanin concentrations increased with VCI level. The median values of Chl-a concentrations were 45, 50, 120, 229, 486 and 8276 $\mu g\,L^{-1}$ for VCI levels 1, 2, 3, 4, 5 and 6, respectively (Fig. 2(a)). However, Chl-a concentration at VCI level 5 varied in a wide range from 391 to 10972 $\mu g\,L^{-1}$. Results of a t-test showed that Chl-a concentrations were significantly different between VCI levels ($P<0.05$), except for levels 1 and 2 ($P>0.05$). Similarly, phycocyanin concentrations were significantly different among VCI levels 3, 4, 5 and 6 ($P<0.05$). The median values of phycocyanin concentrations were 70, 75, 408, 828, 2190 and 28,848 $\mu g\,L^{-1}$ for VCI levels 1, 2, 3, 4, 5 and 6, respectively (Fig. 2(b)).

Fig. 3 shows the in-situ measured reflectance spectra of cyanobacterial blooms at the respective VCI levels. The data were obtained from the observation of Lake Nishiura on August 3, 2012. The reflectance spectra were recalculated to Landsat/ETM+ bands 1–7, except for band 6. Note that the scale of the y-axis is different for VCI levels 1-4 (Figs. 3(a–d)) and levels 5 and 6 (Figs. 3(e and f)). In levels 1 and 2 (Figs. 3(a and b)), where cyanobacteria has not accumulated at the water surface (subsurface blooms; see Figs. A.1(a and b)), the reflectance peaked at band 2, and gradually decreased with increasing wavelengths (bands). The low reflectance at bands 4, 5, and 6 was due to strong absorption of water at such wavelengths. The reflectance at band 4 started to increase in VCI level 3 (Fig. 3(c)), where the cyanobacteria began to aggregate at the water surface (surface scum; see Fig. A(c)). The reflectance at band 4 increased with VCI level, and reached around 0.6 in VCI level 5 (Fig. 3(e)). For VCI level 6, at which the cyanobacteria forms a hyperscum, the reflectance at band 4 decreased, whereas it increased at the visible bands (band 1–3).

3.2. Determination of the FAI threshold for VCI classification

As described above, FAI values were calculated from the reflectance spectra with Eq. (5) and compared to the different VCI levels in order to determine the thresholds (Table 1 and Fig. 4). We also compared the differences in reflectance at bands 3, 4 and 5, which were used for the FAI calculation (Figs. 4(b–d)). The FAI and reflectance at band 4 showed that magnitudes increased with VCI level (Figs. 4(a and c)). However, overlaps were found between VCI levels 5 and 6. A *t*-test indicated that the FAI values were significantly different between VCI levels 2 and 3, 3 and 4, and 4 and 5 ($P<0.05$). They were not, however significantly different between VCI levels 1 and 2 ($P>0.05$, for FAI and band 4, respectively) or between levels 5 and 6 ($P>0.05$, for FAI and band 4, respectively). In contrast, reflectance at band 3 differed significantly from that at VCI levels 5 and 6 (Fig. 4(b)). Reflectances at band 5 were not significantly different from any other VCI level (Fig. 4(d)).

Table 1
In-situ measured pigment concentrations, reflectance, and corresponding FAI values for each observed VCI level. The field investigation was carried out in the Lake Nishiura on August 3, 2012.

VCI Level	Chl-a	Phycocyanine	Reflectance						FAI
	($\mu g\ L^{-1}$)	($\mu g L^{-1}$)	B1	B2	B3	B4	B5	B7	
1	62	119	0.039	0.054	0.043	0.020	0.002	0.001	−0.016
	54	92	0.022	0.029	0.023	0.015	0.007	0.005	−0.006
	53	80	0.025	0.034	0.027	0.016	0.005	0.003	−0.008
2	108	330	0.036	0.052	0.040	0.029	0.005	0.003	−0.005
	110	329	0.035	0.052	0.041	0.027	0.002	0.001	−0.008
	144	402	0.039	0.054	0.042	0.027	0.004	0.003	−0.009
3	174	506	0.034	0.065	0.042	0.052	0.001	0.001	0.017
	131	408	0.043	0.060	0.044	0.046	0.004	0.003	0.009
	192	500	0.038	0.064	0.038	0.060	0.004	0.002	0.028
4	234	834	0.032	0.054	0.034	0.093	0.007	0.001	0.064
	264	674	0.033	0.055	0.035	0.086	0.003	0.000	0.057
	266	980	0.036	0.059	0.036	0.113	0.012	0.005	0.081
5	348	1020	0.040	0.065	0.041	0.169	0.026	0.009	0.131
	815	5245	0.039	0.068	0.039	0.378	0.046	0.011	0.338
	1939	9072	0.056	0.092	0.057	0.518	0.098	0.032	0.454
	5261	19039	0.050	0.083	0.054	0.569	0.098	0.025	0.508
	10972	45222	0.050	0.092	0.053	0.640	0.108	0.026	0.577
6	8278	30178	0.180	0.211	0.180	0.431	0.122	0.041	0.261
	7083	27832	0.103	0.131	0.079	0.508	0.048	0.012	0.434
	9875	28848	0.101	0.138	0.096	0.445	0.058	0.012	0.356

Accordingly, we determined the thresholds between VCI levels by averaging the maximum FAI value at the lower VCI level, and minimum FAI values at the higher VCI level; FAI thresholds were calculated as 0, 0.04 and 0.10 for VCI levels 2 and 3, 3 and 4, and 4 and 5, respectively. We also determined the threshold between VCI levels 5 and 6 using the reflectance at band 3 in the same manner that the FAI thresholds were determined; the thresholds were calculated as 0.07. In addition, we combined VCI levels 1 and 2, because neither FAI nor reflectance values at these levels were significantly different. The classification flowchart for determining VCI level from Landsat/ETM+ images is shown in Fig. 5.

3.3. Estimation of VCI levels from Landsat/ETM+ images

The classification flowchart developed using the in-situ data was applied to three Landsat/ETM+ images from cyanobacteria-dominated periods. Fig. 6 shows the RGB true color images and generated VCI images of Lakes Nishiura, Kitaura, and Hachiro. The cyanobacterial blooms are not clear in the RGB images of Lakes Nishiura and Kitaura on August 21, 2012 or Lake Hachiro on September 13, 2012 (Figs. 6(a and e)). However, the classification maps reveal the presence of cyanobacterial blooms at VCI level 3 (Figs. 6(b and f)). In contrast, the RGB image of Lake Hachiro on

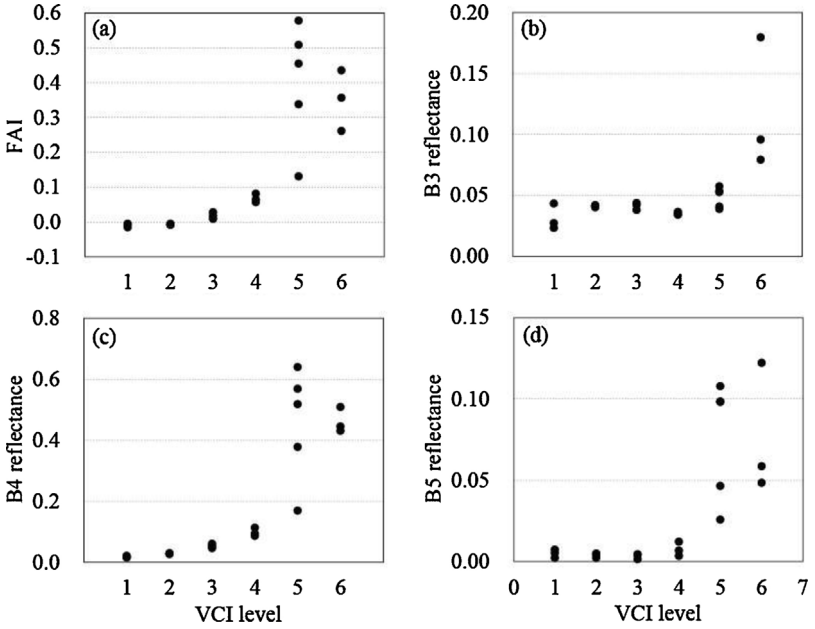

Fig. 4. Changes in the FAI and reflectance values at each VCI level. The used data were collected from the field campaign in Lake Nishiura on August 3, 2012: (a) FAI; (b) reflectance at band 3; (c) reflectance at band 4; (d) reflectance at band 5.

Table 2
Comparison of in-situ observed and satellite-derived VCI levels in Lakes Nishiura, Kitaura and Hachiro. Three Landsat images were acquired on August 21, 28, and September 13, 2012, which were the same dates of the corresponding field surveys. The satellite-derived VCI levels were obtained using the algorithm shown in Fig. 5, and the station numbers are same as those shown in Fig. 1.

Location and date	Station	In-situ	Satellite		
		VCI level	FAI	B3 reflectance	VCI level
Lakes Nishiura and Kitaura August 21, 2012	St.1	5	0.180	0.029	5
	St.2	2	−0.005	–	≤ 2
	St.3	2	−0.015	–	≤ 2
	St.4	2	−0.010	–	≤ 2
	St.6	1	−0.002	–	≤ 2
	St.7	1	−0.001	–	≤ 2
	St.8	4	0.057	–	4
Lake Hachiro August 28, 2012	St.A	3	0.033	–	3
	St.B	4	0.061	–	4
	St.C	5	0.129	0.059	5
	St.D	4	0.057	–	4
	St.E	4	0.058	–	4
Lake Hachiro September 13, 2012	St.A	3	0.019	–	3
	St.B	3	0.018	–	3
	St.C	2	−0.006	–	≤ 2
	St.E	2	−0.008	–	≤ 2
	St.F	2	−0.007	–	≤ 2

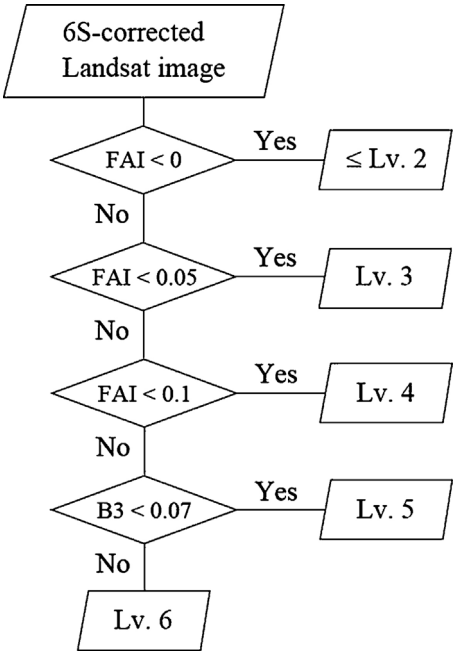

Fig. 5. Classification flowchart for determining VCI level using Landsat/ETM+ images.

August 28, 2012 clearly shows cyanobacteria blooms on the right side of the lake (Fig. 6(c)). The classification map also indicates a high volume of cyanobacterial blooms, up to VCI level 5 (Fig. 6(d)).

The averaged FAI values of the 3×3 window were extracted at each in-situ observation point from the three Landsat/ETM+ images. VCI levels obtained from satellite-derived FAI values were compared with those from in-situ observations (Table 2). There was good accuracy and agreement between VCI levels.

4. Discussion

4.1. The utility of the VCI classification compared with pigment concentrations for monitoring cyanobacterial blooms using satellite images

In this study, we proposed a method for monitoring levels of cyanobacterial blooms using Landsat/ETM+ images. The FAI is first calculated from Landsat/ETM+ images, and then used to classify the volume of cyanobacterial bloom into six VCI levels (Fig. 5). ETM+ band-3 reflectance was used as an additional index for distinguishing between VCI level 5 (surface scum) and 6 (hyperscum). The result of in-situ measurement showed that the FAI increased with Chl-a and phycocyanin concentrations (Fig. 2), implying that the VCI could serve as an alternative index for evaluating levels of cyanobacterial bloom from satellite data. Previous reports of Chl-a concentrations in surface scum varied widely (e.g., 350, 500, and 894 $\mu g\,L^{-1}$ for Jupp et al., 1994; Matthews et al., 2012; Quibell, 1992; respectively), mainly due to the patchiness and heterogeneous density of the scum (Kutser, 2004). Heterogeneity also influences the estimation of Chl-a concentrations from satellite images. The in-situ measured Chl-a concentrations of scum were not comparable to a pixel of satellite images due to the coarse spatial resolution of most satellite sensors (Kutser et al., 2006). In contrast, the VCI represents a range of Chl-a concentration at each level. Therefore, the VCI classification is appropriate for monitoring the development of cyanobacterial blooms using satellite images.

In addition, the VCI can be used to assess how acceptable the lake's condition is to people, because it was developed based on visual appearance. For example, VCI level 3 can be used as a boundary line for acceptability of the lake for recreational uses such as boating, fishing and swimming (Fig. A.2). The amount of Chl-a and phycocyanin does not provide information regarding people's impressions of the lake, although these parameters are important in assessing health risk. World Health Organization (WHO) guidelines also emphasize the importance of visual inspection for cyanobacterial blooms (Bartram and Rees, 2000). They classify lake water quality into three conditions: (1) Secchi transparency of less than 1 m; (2) visible cyanobacteria; and (3) visible cyanobacterial surface scum. The presence of surface scum calls for immediate action to prevent water-contact activities. A visual inspection of surface scum is similar to VCI classification of level 3 or higher. Moreover, VCI level 6, in which cyanobacteria forms hyperscum, is the most serious possible condition of a lake. The disgusting colors and noxious odor of hyperscum result in loss of value for the waterfront. In addition, the aphotic conditions in hyperscum can easily produce the microcystin (toxins produced by *Microcystis* spp.) synthetase (Oberholster et al., 2008). Van Ginkel et al. (2006) reported that the drinking water distribution systems of two towns in South Africa exceeded the WHO guideline of 1 $\mu g\,L^{-1}$ of microcystin during an hyperscum occurrence in the reservoir. Therefore, VCI level 6 can

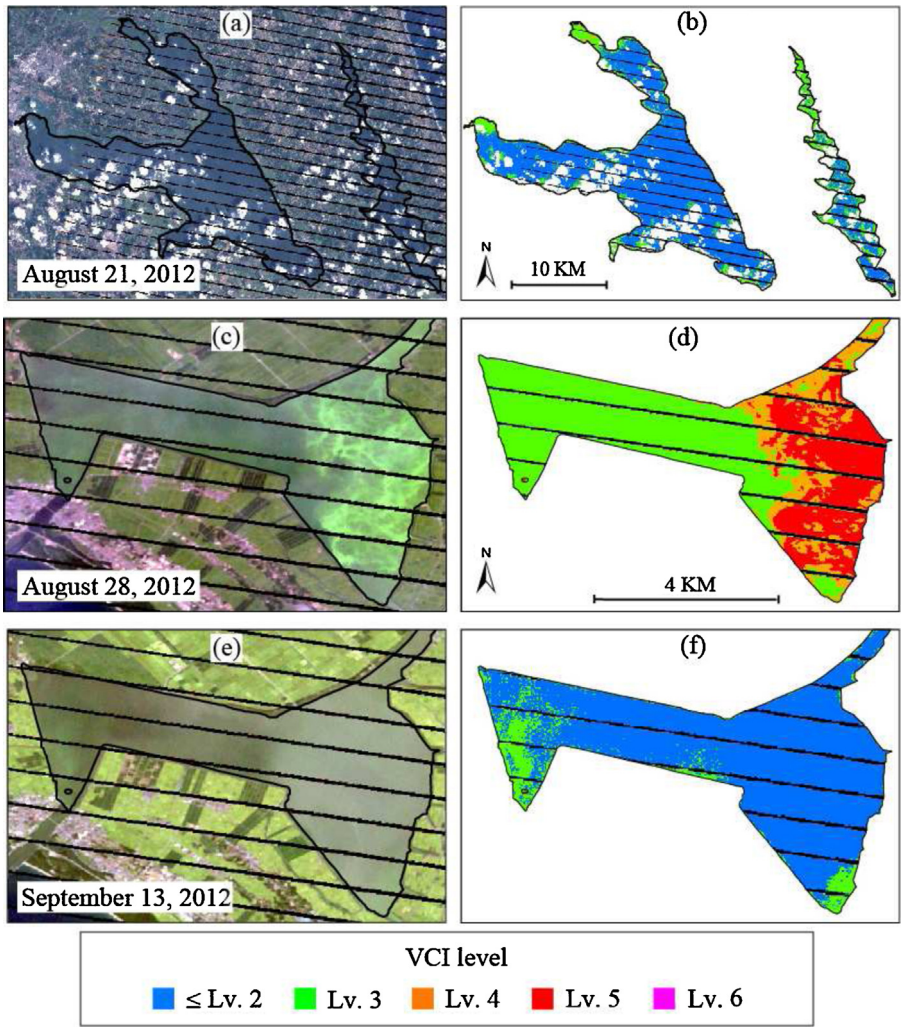

Fig. 6. Landsat/ETM+ images in Lakes Nishiura, Kitaura (Lake Kasumigaura group), and Hachiro during cyanobacteria-dominated periods. The true-color images (a, c, and e) were converted to the VCI images (b, d, and f) using the classification procedure in Fig. 5: (a, b) Lakes Nishiura and Kitaura on August 21, 2012; (c, d) Lake Hachiro on August 28, 2012; (e, f) Lake Hachiro on September 13, 2012.

be used as an indicator of health risks. VCI levels 4 and 5 can also be used as early warning indicators of hyperscum development.

4.2. Advantages of the FAI in monitoring high levels of cyanobacterial surface scum

In remote sensing studies, the extent and volume of cyanobacterial blooms have generally been estimated using pigment concentrations such as Chl-a and phycocyanin. In particular, the MERIS sensor is frequently used to monitor cyanobacterial blooms because of its effective detection bands at 681 and 709 nm of Chl-a fluorescence, and at 620 nm of phycocyanin absorption. However, the characteristic of Chl-a fluorescence peaks is weakened when the cyanobacteria forms surface scums and mats. This is mainly due to the decrease of water absorption at the NIR region with increasing density of cyanobacteria (Ruiz-Verdú et al., 2008; Duan et al., 2012). Table 3 shows the range of Chl-a and phycocyanin concentrations and cell counts of cyanobacterial blooms used in previous remote sensing studies. The maximum Chl-a concentrations in previous studies were lower (<700 $\mu g\,L^{-1}$ maximum for Gómez et al., 2011) than in this study (10,972 $\mu g\,L^{-1}$). Maximum Chl-a concentrations have been reported corresponding to VCI level 2 (70.5 $\mu g\,L^{-1}$ for Binding et al., 2010), level 3 (189.4 $\mu g\,L^{-1}$ for Lunetta et al., 2015), level 4 (290.8 $\mu g\,L^{-1}$ for Media-Cobo et al., 2014), and level 5 (362.5 and <700 $\mu g\,L^{-1}$ for Matthews et al., 2012; and Gómez et al., 2011, respectively).

We calculated the MERIS-derived indices for monitoring cyanobacterial blooms (i.e., MCI, CI and (M9 − M7)/(M9 + M7)) from our in-situ reflectance data in order to compare the upper limits of Chl-a concentration for the respective indices. The in-situ reflectances at 1-nm intervals were recalculated according to each MERIS band reflectance using Eq. (1) with the SRF of each MERIS band. The MCI and CI were calculated using the following equations, respectively (Gower et al., 2005; Wynne et al., 2008):

$$\mathrm{MCI} = R_{\mathrm{M9}} - R_{\mathrm{M8}} + (R_{\mathrm{M10}} - R_{\mathrm{M8}}) \times \frac{(\lambda_{\mathrm{M9}} - \lambda_{\mathrm{M8}})}{(\lambda_{\mathrm{M10}} - \lambda_{\mathrm{M8}})} \quad (6)$$

$$\mathrm{CI} = -\mathrm{SS}_{\mathrm{M8}} \quad (7)$$

where

$$\mathrm{SS}_{\mathrm{M8}} = R_{\mathrm{M8}} - R_{\mathrm{M7}} + (R_{\mathrm{M9}} - R_{\mathrm{M7}}) \times \frac{(\lambda_{\mathrm{M8}} - \lambda_{\mathrm{M7}})}{(\lambda_{\mathrm{M9}} - \lambda_{\mathrm{M7}})} \quad (8);$$

also where M7, M8, M9, M10 are MERIS band 7, 8, 9, and 10, respectively.

Fig. 7 shows the relationships between the four indices and Chl-a concentrations. The MCI are the narrowest range of Chl-a concentrations, because a linear correlation was found between MCI and Chl-a up to 300 $\mu g\,L^{-1}$ of Chl-a concentration (Fig. 7(a)).

Table 3
The range of Chl-a and phycocyanin concentrations and cell count used in the studies for monitoring cyanobacterial blooms with MERIS-derived indices.

Source	Sensor	Index	Chl-a ($\mu g\,L^{-1}$)	Phycocyanin ($\mu g\,L^{-1}$)	Cell count (cells mL^{-1})
Binding et al. (2010)	MERIS	MCI	1.9 – 70.5	–	–
Wynne et al. (2010)	MERIS	CI	–	–	$<1.6 \times 10^7$
Lunetta et al. (2015)	MERIS	CI	0.7 – 189.4	–	$<4.0 \times 10^6$
Matthews et al. (2012)	MERIS	MPH	0.5 – 362.5	–	–
Gómez et al. (2011)	MERIS	(M9 – M7)/(M9 + M7)	<700	<800	–
Medina-Cobo et al. (2014)	MERIS	(M9 – M7)/(M9 + M7)	0.9 – 290.8	17.1 – 456.51	$<1.0 \times 10^7$
This study	ETM+	FAI	53 – 10972	80 – 45222	–

The CI and (M9 – M7)/(M9 + M7) showed linear correlations below 1000 $\mu g\,L^{-1}$ of Chl-a concentration (Figs. 7(b and c)). The MPH had characteristics similar to the CI. These upper limits of Chl-a concentration almost corresponded to the maximum Chl-a concentrations in previous studies (see Table 3). In contrast, the FAI showed a linear correlation in spite of the higher Chl-a concentration (>1000 $\mu g\,L^{-1}$) except for hyperscum (Fig. 7(d)). This was because the SWIR region, which is used to calculate the FAI, is more influenced by water absorption than by the NIR region; therefore, the height of the peak at the NIR region is highlighted by the baseline. In addition, the FAI can be applied to many medium-resolution satellite sensors with SWIR bands (e.g., Terra/ASTER; EO-1/ALI; SPOT/HRVIR and HRG; and ResourceSat/LISS-III); this makes it possible to monitor cyanobacterial blooms in small lakes and ponds. However, the FAI could not detect the peak in the case of low Chl-a concentration (<150 $\mu g\,L^{-1}$) in which the cyanobacteria formed subsurface blooms (VCI level 1 and 2) because of the coarse spectral resolution of the NIR band in ETM+ sensor. Therefore, the MERIS-derived indices are more suitable for monitoring cyanobacterial blooms in large-scale water areas when the cyanobacteria forms subsurface blooms and thin surface scum (<1000 $\mu g\,L^{-1}$ of Chl-a concentration). In contrast, the FAI may be useful for monitoring surface scum with a higher range of Chl-a concentration in small-to-large-scale water areas.

Meanwhile, none of the four indices could distinguish hyperscum from surface scum. Although hyperscum did not appear in our three Landsat images, the in-situ reflectance data indicated that Landsat/ETM+ band-3 reflectance was significantly different

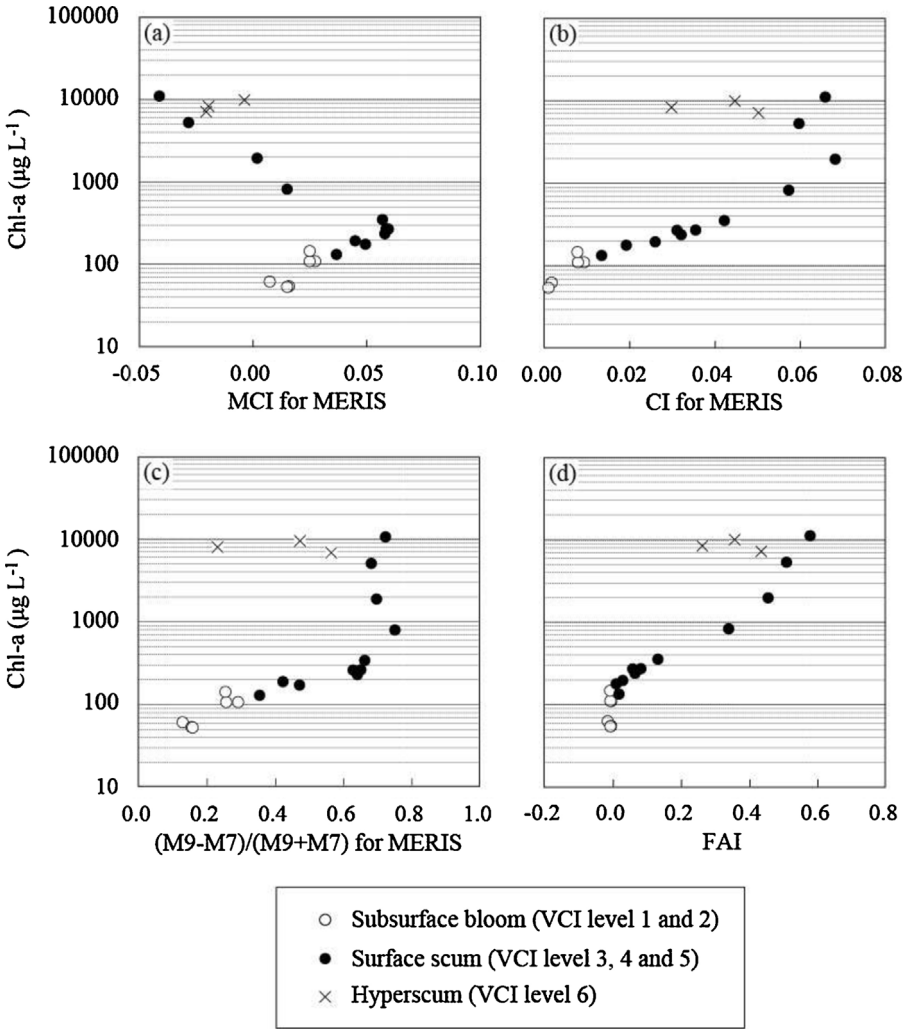

Fig. 7. Relationships between four indices for monitoring cyanobacterial blooms and Chl-a concentration. The MERIS band reflectances for calculating each index were simulated from in-situ measured reflectances at 1 nm intervals (field campaign on August 3, 2012) using Eq. (1): (a) MCI; (b) CI; (c) normalized band ratio index of (M9 – M7)/(M9 + M7); (d) FAI.

between them (Fig. 4(b)). Oberholster et al. (2008) also qualitatively detected hyperscum in Lake Hartbeespoort, South Africa, using a Landsat/TM image. They reported that hyperscum had a distinctive white pattern in the image because the upper layer of the cyanobacteria cells was exposed to photo-oxidizing conditions under high light intensity, resulting in bleaching of the pigments. Our in-situ data showed that the reflectances at visible bands in hyperscum were much higher than in other forms of cyanobacterial blooms (Fig. 3). This result shows that reflectances at visible wavelengths are effective in distinguishing hyperscum from surface scum.

4.3. Toward a practical use for monitoring cyanobacterial blooms from satellite images using the VCI

There are three practical concerns with regards to using the VCI to monitor cyanobacterial blooms from satellite images. First, accurate atmospheric corrections are necessary in order to adjust the FAI thresholds for the VCI classification. Atmospheric radiative transfer codes such as 6S and MODTRAN (Berk et al., 2006) are useful when cyanobacteria forms surface scum. This is because most of the atmospheric models designed for oceans assume negligible water reflectance in the NIR region (Hu, 2009). Second, other algal blooms such as dinoflagellates and diatoms must be distinguished from cyanobacterial blooms. Most of satellite sensors than can calculate the FAI (e.g., Terra/MODIS, Terra/ASTER, and Landsat/TM and ETM+) do not have a band around 620 nm for phycocyanin detection. The satellite sensors equipped with such detection bands should be used when there is no in-situ information about dominant phytoplankton species during observation. Third, satellite sensors with high spatial and temporal resolution are required because of the spatiotemporal variability of cyanobacterial blooms. The coarse temporal resolution of Landasat/ETM+ (16 days) may mean that opportunities to manage health risks for water users will be lost. The next generation satellites, such as the sentinel-2 (10–60 m of spatial resolution, 5 days of the repeat cycle with a constellation of two satellites, and 13 spectral bands in visible, NIR and SWIR regions; Drusch et al., 2012), will have great potential for monitoring cyanobacterial blooms.

5. Conclusion

In this study, we proposed a method for monitoring the levels of cyanobacterial blooms using Landsat/ETM+ images. The FAI is first calculated from Landsat/ETM+ images, and then used to classify the volume of cyanobacterial blooms into six VCI levels. The VCI classification system is appropriate when cyanobacteria form surface scums and hyperscum in the lake. The simulation using in-situ reflectance data showed that the FAI is more suitable for monitoring cyanobacterial blooms at extremely high Chl-a concentrations (>1000 $\mu g\,L^{-1}$), compared with the MERIS-derived indices such as MCI and CI. There are three practical concerns for temporal monitoring of cyanobacterial blooms from satellite images with the VCI: 1) accurate atmospheric corrections; 2) distinction of cyanobacterial blooms from other algal blooms; and 3) satellite sensors with a high spatial and temporal resolution.

Acknowledgements

We sincerely thank Dr. Hiroya Yamano and Dr. Akihide Kamei of Japan's National Institute for Environmental Studies (NIES) for the use of the FieldSpec FR spectroradiometer. We also would like to thank two anonymous reviewers for their helpful comments and suggestions. This research was supported in part by the Global Environment Research Fund (S-9) of Japan's Ministry of the Environment, and by Grants-in-Aid for Scientific Research from Japan's Ministry of Education, Culture, Sports, Science, and Technology (MEXT) (Nos. 23404015 and 25420555).

Appendix Appendix A. The visual cyanobacteria index (VCI): a simple index for in-situ visual interpretation of cyanobacterial blooms

Appendix A. The visual cyanobacteria index (VCI): a simple index for in-situ visual interpretation of cyanobacterial blooms

The visual cyanobacteria index (VCI) proposed by Aizaki et al. (1995a) is an index for monitoring bloom levels by visual interpretation. The advantage of the VCI is that everyone can observe the status of the cyanobacterial blooms in a lake without special skills or instruments. It has been widely used by Japan's local governments to manage the quality of inland waters. The VCI classifies cyanobacterial blooms into the six levels of aggregation described below:

Level 1: Blooms cannot be observed visually without tools such as a phytoplankton net or a white container (Fig. A.1(a))

Level 2: The bloom spreads slightly as filaments, and can be observed visually (Fig. A.1(b));

Level 3: The bloom spreads on the water surface and forms patches and scums (Fig. A.1(c));

Level 4: The bloom covers the water surface as thin film (Fig. A.1(d));

Level 5: The bloom covers the water surface as thick mat (Fig. A.1(e));

Level 6: The cyanobacterial mat is crusted and releases a strong odor; at this level it is called a hyperscum (Zohary and Breen, 1989). The color can often change from green to white, purple or blue (Fig. A.1(f)).

Since the VCI is closely related to the lake scenery, it can be used to evaluate the acceptability of the water for recreational and/or drinking uses. Aizaki et al. (1995b) also investigated the relationships between the lake landscape and the acceptability of water based on a questionnaire survey with the photographs in Fig. A.1. In this survey, a photograph of the clearest lake in Japan (Lake Mashu: >20 m transparency) was added as an example of a lake without cyanobacteria (level 0) (Fig. A.1(g)). The questions were: (Q1) how do you feel about the photograph? (Q2) how do you feel about this lake as a drinking-water source? (Q3) does the photograph make you want to go boating? (Q4) does it make you want to go fishing? (Q5) would you want to play in the water? (Q6) would you want to go walking around the lakeside? (Fig. A.2). In the first question, the percentage responding "clear" decreased with increasing VCI level, and was approximately zero at anything over VCI level 3. In contrast, the percentage that responded "disgusting" increased from VCI level 4 on. Similarly, the number of people who would hesitate to use the water as a drinking source increased with VCI level (Q2 in Fig. A.2). In the questions about water recreational activities (Q3–6 in Fig. A.2), the percentage responding, "yes" rapidly decreased around VCI level 3. This result indicates that VCI level 3 is the limit for people's acceptance of a body of water for recreational uses.

Although the VCI is a convenient index for monitoring cyanobacterial blooms, the evaluation sometimes depends on the observer. Fig. A.3 shows the results of VCI evaluations of cyanobacterial blooms in Lake Nishiura by local residents. The photographs in Fig. A.1 were used as a standard of evaluation. The higher frequency is concentrated in one level or its surrounding levels, meaning that the VCI evaluation did not vary widely among the observers. However, an irregular distribution is found in center of the lake on 21 July (Fig. A.3(b)). Thus, simple training is necessary for observers to have a common understanding of how to use the VCI for monitoring cyanobacterial blooms.

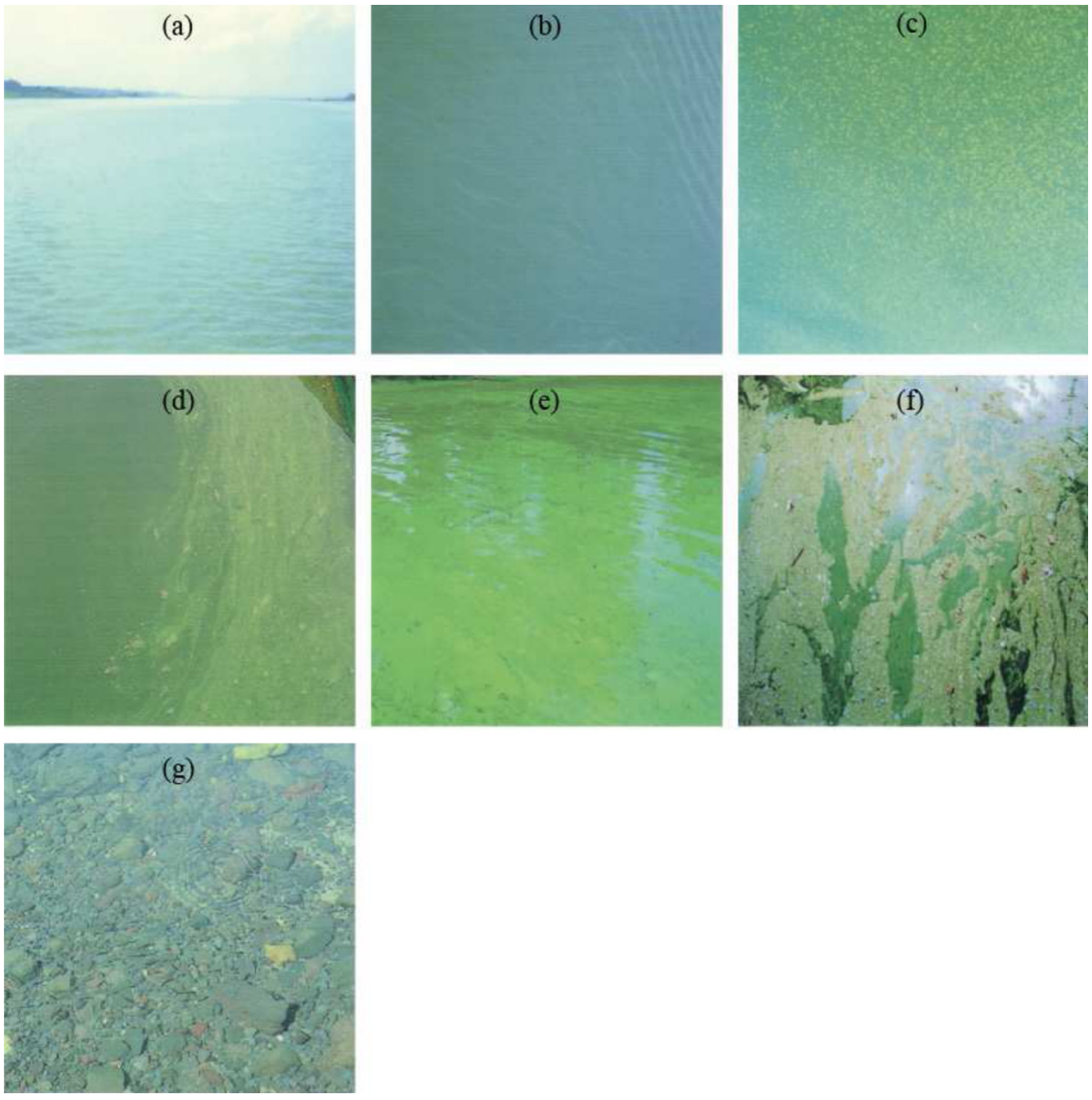

Fig. A.1. Photographs of various levels of cyanobacterial blooms in Lake Nishiura (west part of Lake Kasumigaura), Japan. The blooms were classified into six levels based on visual appearance: (a) Level 1; (b) level 2; (c) level 3; (d) level 4; (e) level 5; (f) level 6. (g) A photograph of the clearest lake in Japan (Lake Mashu; >20 m transparency) with no cyanobacteria was shown as level 0. The level 0 photograph was only used for a questionnaire about lake amenities (see Fig. A.2). All the photographs were from Aizaki et al. (1995a).

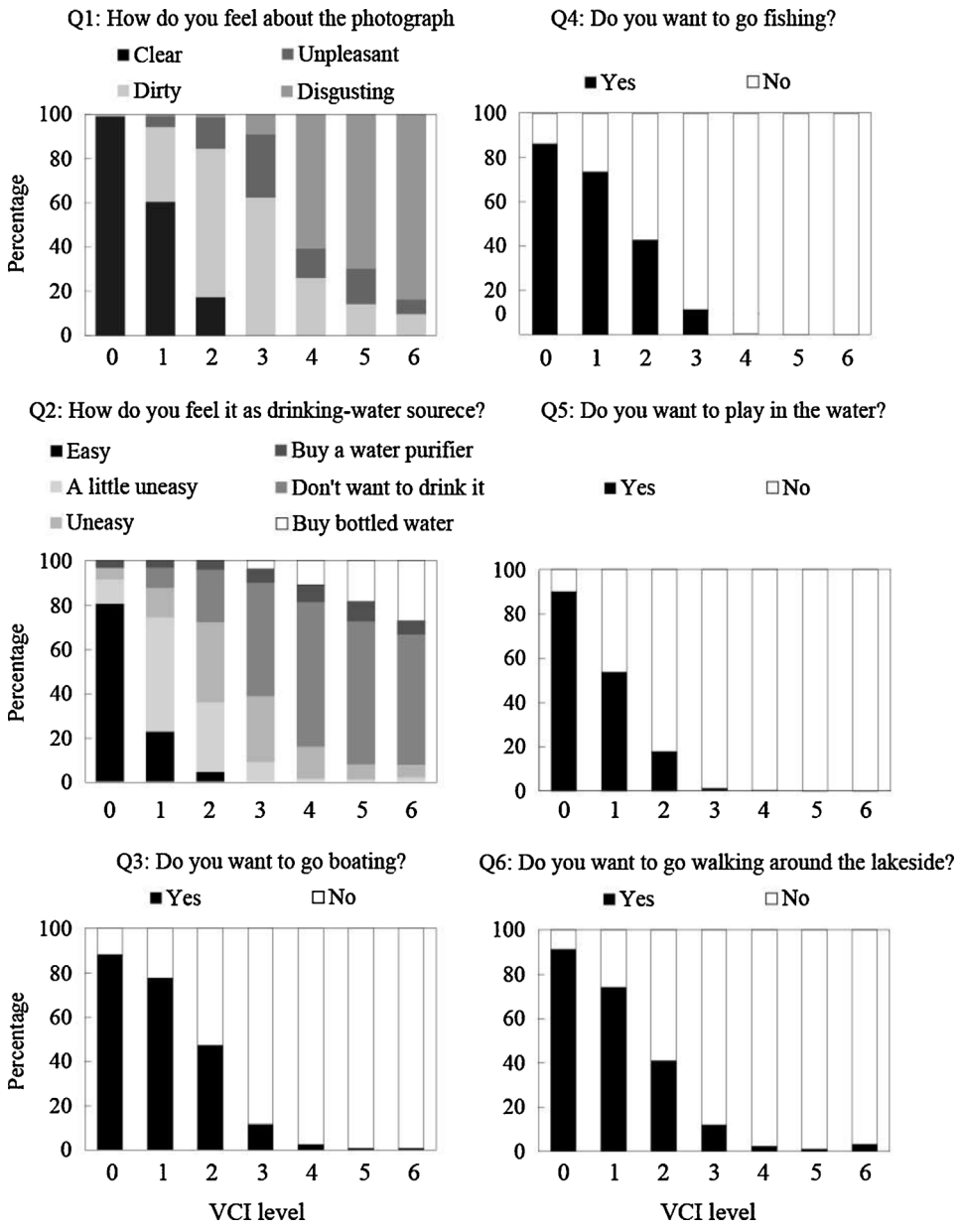

Fig. A.2. Results of the questionnaire about water quality and water use using the photographs of the VCI ($N = 253$). The data were modified from Aizaki et al. (1995b).

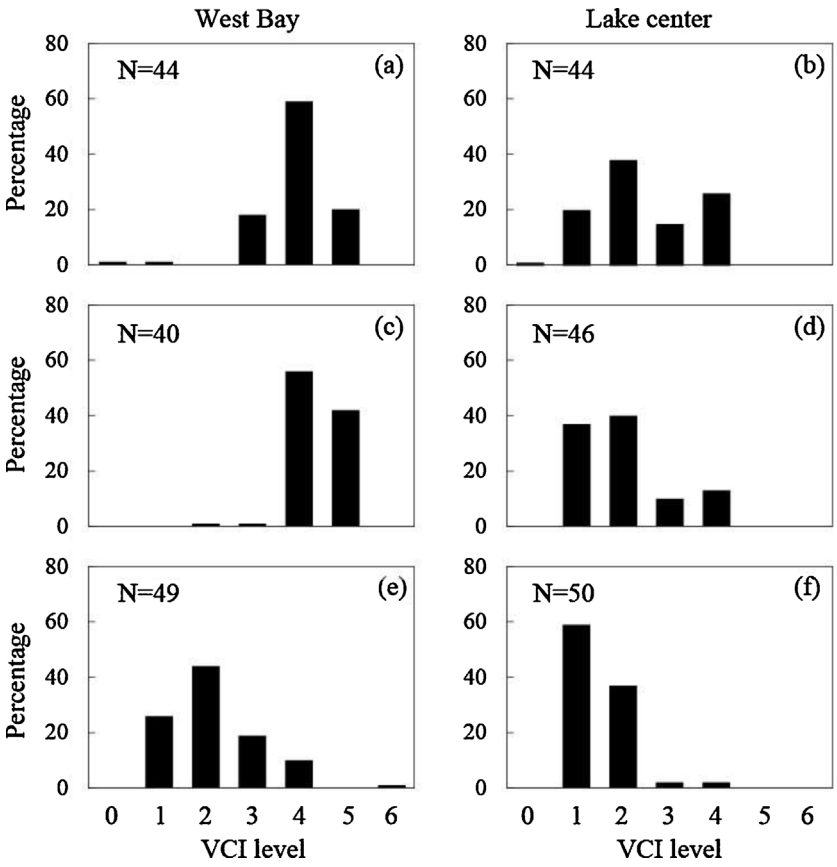

Fig. A.3. Evaluation of cyanobacterial blooms in Lake Nishiura by local residents using the VCI: (a, b) July 21, 1992; (c, d) July 28, 1992; and (e, f) August 12, 1992. The data were from Aizaki et al. (1995b).

References

Aizaki, M., Fukushima, T., Takagi, H., Kitamura, H., 1995a. Evaluation of Lake Kasumigaura, Japan, using a landscape index for cyanobacterial bloom. In: Aizaki, M., Fukushima, T. (Eds.), Aoko (Water-blooms of Blue-green Algae); Measurement, Occurrence, and Factors on Its Growth. National Institute for Environmental Studies, Tsukuba, Japan, pp. 33–39 (in Japanese).

Aizaki, M., Fukushima, T., Kitamura, H., Ohashi, H., 1995b. What is criteria for cyanobacterial bloom? An analysis of questionnaire investigation using the visual cyanobacterial index. In: Aizaki, M., Fukushima, T. (Eds.), Aoko (Water-blooms of Blu–green Algae); Measurement, Occurrence, and Factors on Its Growth. National Institute for Environmental Studies, Tsukuba, Japan, pp. 40–48 (in Japanese).

Bartram, J., Carmichael, W.W., Chorus, I., Jones, G., Skulberg, O.M., 1999. Introduction. In: Chorus, I., Bartram, J. (Eds.), Toxic Cyanobacteria in Water: A Guide to Their Public Health Consequences, Monitoring and Management. E & FN Spon, London and New York, pp. 1–14.

Bartram, J., Rees, G. (Eds.), 2000. London, E & FN Spon Press, London and New York.

Berk, A., Anderson, G.P., Acharya, P.K., Bernstein, L.S., Muratov, L., Lee Fox, J.M., Adler-Golden, S.M., Chetwynd, J.H., Hoke, M.L., Lockwood, R.B., Gardner, J.A., Cooley, T.W., Borel, C.C., Lewis, P.E., Shettle, E.P., 2006. MODTRAN5: 2006 Update. Proc. SPIE 6233, 62331F.

Binding, C.E., Greenberg, T.A., Jerome, J.H., Bukata, R.P., Letourneau, G., 2010. An assessment of MERIS algal products during an intense bloom in Lake of the Woods. J. Plankton Res. 33, 793–806.

Blondeau-Patissier, D., Gower, J.F.R., Dekker, A.G., Phinn, S.R., Brando, V.E., 2014. A review of ocean color remote sensing methods and statistical techniques for the detection: mapping and analysis of phytoplankton blooms in coastal and open oceans. Prog. Oceanogr. 123, 123–144.

Carpenter, S.R., Caraco, N.F., Correll, D.L., Howarth, R.W., Sharpley, A.N., Smith, V.H., 1998. Nonpoint pollution of surface waters with phosphorus and nitrogen. Ecol. Appl. 8 (3), 559–568.

Codd, G.A., 2000. Cyanobacterial toxins, the perception of water quality, and the prioritization of eutrophication control. Ecol. Eng. 16 (1), 51–60.

Dash, P., Walker, N.D., Mishra, D.R., Hu, C., Pinckney, J.L., D'sa, E.J., 2011. Estimation of cyanobacterial pigments in a freshwater lake using OCM satellite data. Remote Sens. Environ. 115, 3409–3423.

Dokulil, M., Teubner, K., 2000. Cyanobacterial dominance in lakes. Hydrobiologia 438, 1–12.

Drusch, M., Del Bello, U., Carlier, S., Colin, O., Fernandez, V., Gascon, F., Hoersch, B., Isola, C., Laberinti, P., Martimort, P., Meygret, A., Spoto, F., Sy, O., Marchese, F., Bargellini, P., 2012. Sentinel-2: ESA's optical high-resolution mission for gmes operational service. Remote Sens. Environ. 120, 25–36.

Duan, H., Ma, R., Hu, C., 2012. Evaluation of remote sensing algorithms for cyanobacterial pigment retrievals during spring bloom formation in several lakes of East China. Remote Sens. Environ. 126, 126–135.

Gómez, J.A.D., Alonso, C.A., García, A.A., 2011. Remote sensing as a tool for monitoring water quality parameters for Mediterranean Lakes of European Union water framework directive (WFD) and as a system of surveillance of cyanobacterial harmful algae blooms (SCyanoHABs). Environ. Monit. Assess. 181, 317–334.

Gower, J., King, S., Borstad, G., Brown, L., 2005. Detection of intense plankton blooms using the 709 nm band of the MERIS imaging spectrometer. Int. J. Remote Sens. 26, 2005–2012.

Hino, S., Takano, K., 1995. Estimation of cyanobacteria dominance in lakes. In: Aizaki, M., Fukushima, T. (Eds.), Aoko (Water-blooms of Blue–green Algae); Measurement, Occurrence, and Factors on Its Growth. National Institute for Environmental Studies, Tsukuba, Japan, pp. 15–23 (in Japanese).

Hu, C., 2009. A novel ocean color index to detect floating algae in the global oceans. Remote Sens. Environ. 113 (10), 2118–2129.

Hu, C., He, M.-X., 2008. Origin and offshore extent of floating algae in Olympic sailing area. EOS, Trans. Am. Geophys. Union 89 (33), 302–303.

Jupp, D.L.B., Kirk, J.T.O., Harris, G.P., 1994. Detection: identification and mapping of cyanobacteria – using remote sensing to measure the optical quality of turbid inland waters. Aust. J. Mar. Freshwater Res. 45, 801–828.

Kahru, M., Horstmann, U., Rud, O., 1994. Satellite detection of increased cyanobacteria blooms in the baltic sea: natural fluctuation or ecosystem change? Ambio 23 (8), 469–472.

Kutser, T., 2004. Quantitative detection of chlorophyll in cyanobacterial blooms by satellite remote sensing. Limnol. Oceanogr. 49, 2179–2189.

Kutser, T., Metsamaa, L., Strömbeck, N., Vahtmäe, E., 2006. Monitoring cyanobacterial blooms by satellite remote sensing. Estuarine Coastal Shelf Sci. 67, 303–312.

Lobo, F.L., Barbosa, C.C., Novo, E.M.M.L., Yunes, J.S., 2009. Mapping potential cyanobacterial bloom using Hyperion/EO-1 data in Patos Lagoon estuary. Phys. Limnol. 21, 299–308.

Lunetta, R.S., Schaeffer, B.A., Stumpf, R.P., Keith, D., Jacobs, S.A., Murphy, M.S., 2015. Evaluation of cyanobacteria cell count detection derived from MERIS imagery across the eastern USA. Remote Sens. Environ. 157, 24–34.

Matthews, M.W., 2014. Eutrophication and cyanobacterial blooms in South African inland waters: 10 years of MERIS observations. Remote Sens. Environ. 155, 161–177.

Matthews, M.W., Bernard, S., Robertson, L., 2012. An algorithm for detecting trophic status (chlorophyll-a) cyanobacterial-dominance, surface scums and floating vegetation in inland and coastal waters. Remote Sens. Environ. 124, 637–652.
McKinna, L.I.W., Furnas, M.J., Ridd, P.V., 2011. A simple, binary classification algorithm for the detection of Trichodesmium spp. within the great barrier reef using MODIS imagery. Limnol. Oceanogr. Methods 9, 50–66.
Medina-Cobo, M., Domínguez, J.A., Quesada, A., de Hoyos, C., 2014. Estimation of cyanobacteria biovolume in water reservoirs by MERIS sensor. Water Res. 63C, 10–20.
Mishra, S., Mishra, D.R., 2014. A novel remote sensing algorithm to quantify phycocyanin in cyanobacterial algal blooms. Environ. Res. Lett. 9 (11), 114003.
Mobley, C.D., 1999. Estimation of the remote-sensing reflectance from above-surface measurements. Appl. Opt. 38 (36), 7442–7455.
Mueller, J.L., Davis, C., Arnone, R., Frouin, R., Carder, K., Lee, Z.P., 2000. Above-water radiance and remote sensing reflectance measurements and analysis protocols. In: Ocean Optics Protocols for Satellite Ocean Color Sensor Validation Revision 2. National Aeronautical and Space Administration, Greenbelt, Maryland (pp. 98-107).
Oberholster, P.J., Cloete, T.E., van Ginkel, C., Botha, A.M., Ashton, P.J., 2008. The use of remote sensing and molecular markers as early warning indicators of the development of cyanobacterial hyperscum crust and microcystinproducing genotypes in the hypertrophic Lake Hartebeespoort, South Africa. Council for Scientific and Industrial Res. 1–15.
Pretty, J.N., Mason, C.F., Nedwell, D.B., Hine, R.E., Leaf, S., Dils, R., 2003. Environmental costs of freshwater eutrophication in England and Wales. Environ. Sci. Technol. 37 (2), 201–208.
Quibell, G., 1992. Estimating chlorophyll concentrations using upwelling radiance from different freshwater algal genera. Int. J. Remote Sens. 13, 2611–2621.
Ruiz-Verdú, A., Simis, S.G.H., de Hoyos, C., Gons, H.J., Pena- Martinez, R., 2008. An evaluation of algorithms for the remote sensing of cyanobacterial biomass. Remote Sens. Environ. 2008 (112), 3996–4008.
Sato, A., 1990. The agriculture and characteristics of chemical and physical properties of heavy clay soil in the Hachiro-gata polder. J. Clay Sci. Soc. Jpn. 30 (2), 115–125 (In Japanese with English abstract).
SCOR-UNESCO, 1966. Determination of photosynthetic pigment in seawater. Monographs on Oceanographic Methodology, 1. UNESCO, Paris (pp. 11–18).
Simis, S.G.H., Peters, S.W.M., Gons, H.J., 2005. Remote sensing of the cyanobacterial pigment phycocyanin in turbid inland water. Limnol. Oceanogr. 50, 237–245.
Smith, V.H., Schindler, D.W., 2009. Eutrophication science: where do we go from here? Trends Ecol. Evol. 24 (4), 201–207.
Song, K., Li, L., Tedesco, L.P., Li, S., Hall, B.E., Du, J., 2014. Remote quantification of phycocyanin in potable water sources through an adaptive model. ISPRS J. Photogramm. Remote Sens. 95, 68–80.
Storey, J., Scaramuzza, P., Schmidt, G., Barsi, J., 2005. Landsat 7 scan line corrector-off gap-filled product development. Proc. 2005 ASPRS, 23–27.
Subramaniam, A., Brown, C.W., Hood, R.R., Carpenter, E.J., Capone, D.G., 2002. Detecting *Trichodesmium* blooms in SeaWiFS imagery. Deep. Sea Res. Part II 49, 107–121.
Van Ginkel, C.E., Silberbauer, M.J., Plessis, S., Carelsen, C.I.C., 2006. Monitoring microcystin toxin and chlorophyll in five South African impoundments. Verh. Internat. Verein. Limnol. 29, 1611–1616.
Vermote, E.F., Tanre, D., Deuze, J.L., Herman, M., Morcette, J.J., 1997. Second simulation of the satellite signal in the solar spectrum, 6S: an overview. IEEE Trans. Geo. Remote Sens. 35 (3), 675–686.
Vincent, R.K., Qin, X., McKay, R.M.L., Miner, J., Czajkowski, K., Savino, J., Bridgeman, T., 2004. Phycocyanin detection from LANDSAT TM data for mapping cyanobacterial blooms in Lake Erie. Remote Sens. Environ. 89, 381–392.
Wynne, T.T., Tomlinson, M.C., Warner, R.A., Tester, P.A., Dyble, J., Fahnensteil, G.L., 2008. Relating spectral shape to cyanobacterial blooms in the Laurentian Great Lakes. Int. J. Remote Sens. 29, 3665–3672.
Wynne, T.T., Stumpf, R.P., Tomlinson, M.C., Dyble, J., 2010. Characterizing a cyanobacterial bloom in Western Lake Erie using satellite imagery and meteorological data. Limnol. Oceanogr. 55, 2025–2036.
Zohary, T., Breen, C.M., 1989. Environmental factors favouring the formation of Microcystis aeruginosa hyperscums in a hypertrophic lake. Hydrobiologia 178, 179–192.